KSCE Journal of Civil Engineering (2024) 28(5):1836-1852
DOI 10.1007/s12205-024-0020-0

pISSN 1226-7988, eISSN 1976-3808
www.springer.com/12205

Structural Engineering

FE Analysis on Size Effect in Torsional Behavior of Rectangular RC Beams with and Without FRP Strengthening

Mojtaba Shokri[a], **Mahmoud Edalati**[b], **S. Mohammad Mirhosseini**[a], **and Ehsanollah Zeighami**[a]

[a]*Dept. of Civil Engineering, Arak Branch, Islamic Azad University, Arak 38135-567, Iran*
[b]*Dept. of Civil Engineering, Ilam University, Ilam 69315-516, Iran*

ARTICLE HISTORY

Received 19 February 2023
Revised 27 September 2023
Accepted 7 December 2023
Published Online 15 February 2024

KEYWORDS

RC beam
Torsion
Fiber-reinforced polymer (FRP)
Finite element
Size effect

ABSTRACT

Although torsion is usually considered a secondary consideration in structural design, it can lead to failures, especially in structures with irregular geometry exposed to seismic forces or in unique situations. While some studies have explored the size effect on the torsional behavior of RC beams, none have addressed the impact of reinforcement. This paper investigates the size effect on the torsional behavior of RC beams with varying reinforcement ratios, including both FRP sheets and steel rebars. In this study, the torsional behavior of reinforced concrete (RC) beams with and without FRP strengthening was investigated numerically. Modeling was carried out by Finite element (FE) software ABAQUS and validated using experimental data from literature. The torsional behavior of 24 models with differences in cross-section size and reinforcement ratio were investigated. Concrete damage plasticity, Hashin damage criteria, and von Mises stress were used to investigate the damage in concrete, FRP, and steel, respectively. The cracking torsional moment, ultimate torsional moment, and torque-twist curve of the beams were evaluated and presented. The results indicated the presence of a significant size effect in the torsional strength of beams. After reinforcing the beams with FRP fabrics, the average cracking moment increased by a range of 1.72% to 36% across different groups of beams. An 8.2% increase in ultimate strength is observed with just a 0.4% rise in the FRP strengthening ratio. Post-cracking behavior was seen in 8 models with adequate steel and FRP reinforcement ratio.

1. Introduction

Concrete members such as beams or columns are designed to resist bending moments, shear forces, axial forces, and torsional moments or a combination of them. Torsion is not the major concern in beams and it is considered a secondary effect compared with shear and flexural effects. However, torsional failure may occur due to irregular geometry of structure under seismic load or in some certain cases such as spandrels, curved beams in structures, and eccentrically loaded girders in bridges (Alabdulhady and Sneed, 2019). Torsional strength in usual RC beams consists of strength in concrete and steel reinforcement and strengthening the beams by FRP will provide additional torsional strength for the member. Retrofitting and rehabilitation may become vital in existing structures due to some reasons like aging, change in use, errors in designing and/or construction, earthquake damage (Panchacharam and Belarbi, 2002). The utilization of Fiber Reinforced Polymer (FRP) materials in the enhancement of concrete structures has emerged as a significant area of research and application in the field of civil engineering. The inherent advantages offered by FRP materials, including but not limited to their remarkable mechanical properties, resistance to corrosion, and relatively low weight, have catalyzed their extensive adoption in structural engineering endeavors (Zou et al., 2021). One of the primary motivations for the integration of FRP materials into concrete structures is the imperative need for structural rehabilitation and strengthening. Aging infrastructure, changes in structural usage, design deficiencies, and the impact of environmental factors necessitate the enhancement of existing concrete members. FRP materials present a versatile and effective solution for these

CORRESPONDENCE Mahmoud Edalati m.edalati@ilam.ac.ir Dept. of Civil Engineering, Ilam University, Ilam 69315-516, Iran

rehabilitation efforts. Furthermore, FRP materials provide an invaluable means of addressing challenges associated with conventional reinforcement materials, such as steel. Unlike steel, FRP materials are non-corrosive, eliminating the risk of corrosion-induced deterioration in concrete structures. This characteristic is especially advantageous in aggressive environments, where exposure to moisture, chloride ions, or other corrosive agents can compromise the structural integrity of conventional reinforced concrete elements (Bakis et al., 2002). Additionally, the lightweight nature of FRP materials eases handling and installation, reducing labor and transportation costs. Moreover, FRP materials offer a high strength-to-weight ratio, enabling the development of slender and aesthetically pleasing structural members while maintaining robust structural performance. While the adoption of FRP materials in concrete structures has witnessed substantial growth, challenges persist. These include the initial cost of FRP materials, limited ductility compared to traditional steel reinforcement, and relatively low modulus of elasticity. These limitations necessitate a nuanced consideration of FRP materials in the context of specific engineering applications, taking into account their unique attributes and limitations (Cheng and Karbhari, 2006; Grace et al., 2012). The behavior of RC beams strengthened with fibers has become an interesting issue for researchers in the past decades. Flexural behavior of FRP-confined RC beams has been investigated in several researches (Kara and Ashour, 2012; Önal et al., 2014; Pawłowski and Szumigała, 2015; Lee et al., 2020; Al-Rousan and Issa, 2017; Chen et al., 2018). Meanwhile, some others conducted investigations on the shear behavior of FRP-confined RC beams (Teng et al., 2004; Godat et al., 2007; Manos et al., 2014; Hussain and Pimanmas, 2015; Jumaa and Yousif, 2019; Zheng et al., 2020). Naderpour et al. (2020) conducted a study employing Artificial Neural Networks (ANNs) to develop a highly accurate predictive equation for the shear strength of concrete beams reinforced with FRP bars, surpassing conventional conservative models. Also, there are some studies on axial behavior of FRP-confined RC beams (Akguzel, 2011; Agarwal et al., 2014; Sharaky et al., 2018; Raza and Ahmad, 2020; Yu et al., 2021) but there is much work to do in the field of torsional behavior.

Ghobarah et al. (2002) were one the first to investigate the torsional resistance of RC beams strengthened by FRP fabrics. In that experimental study, different configurations of FRP wrapping were tested on 11 beams. The result showed that full wrapping performs better than using stirrup and the 45° spiral wrap is a better way to upgrade the torsional resistance of RC beams than vertical stirrups. Panchacharam and Belarbi (2002) conducted an experimental study to question the effect of some variables on the torsional strength of FRP strengthened RC beams. The variables considered to investigate were the orientation of fiber, 3 faces versus 4 faces strengthening and fully and completely wrapped versus U-wrap, and the number of plies placed in wrapping. The results showed significant improvement in cracking and ultimate strength of FRP strengthened RC beams and a comparison was made for different types of strengthening. A total number of 39 RC beams were cast and strengthened by FRP in a study conducted by Tibhe and Rathi (2016). CFRP and GFRP fabrics were used with various wrapping patterns. A comparison was made between CFRP and GFRP failure modes and various wrapping results were presented.

There are a few FE studies on the torsional behavior of FRP strengthened RC beams. Analytical and numerical studies were conducted by Ganganagoudar et al. (2016) to investigate the torque-twist behavior of an FRP strengthened RC beam. The results from analytical and numerical were in good agreement with test data so both approaches were found to be useful in predicting the behavior of FRP strengthened RC beam. The main outcomes of the study were that FRP strengthening will increase the post-cracking stiffness, ultimate strength and localized the damage. In contrast to this study, Ganganagoudar et al.'s paper focuses on investigating beam torque-twist behavior but does not include a parametric study to assess the effects of FRP strengthening, reinforcement ratio, and size effect. A numerical study was carried out using FE software ABAQUS by Majed et al. (2021). The authors used experimental data to validate a numerical model to investigate the cracking and torsional behavior of FRP strengthened RC beam. They examined the effect of the number of FRP fabrics, compressive strength of concrete, and FRP strip orientations on the torsional failure of RC beam with and without FRP strengthening. The results showed that increasing the concrete compressive strength and number of FRP plies will cause a major increase in the torsional capacity. Hii and Al-Mahaidi (2006) conducted experimental and numerical studies on FRP strengthened RC beams and used the experimental data to validate the modeling made by DIANA software. Predicted Torsional behavior from FE analysis was in good agreement with experimental data in terms of cracking in concrete, yielding in steel, the rupture in FRP, and torque-twist curve of specimens. Mirrashid and Naderpour (2021) conducted a comprehensive review, which examined the application of soft computing (SC) methods in predicting the behavior of concrete structural elements between 2010 and 2020. Their study underscores the effectiveness of these methods while highlighting the need for improved documentation in existing research. Additionally, in another study by Mirrashid and Naderpour (2020), damage states for RC building elements such as beams, columns, and joints were introduced using pushover analysis and soft computing techniques. This research provides a more detailed description of damaged RC frames and highlights their potential for seismic studies.

A numerical solution was presented by Ameli et al. (2007) to predict the torsional behavior of RC beam strengthened by FRP. They used ANSYS software for FE modeling and questioned the effect of FRP configuration on ultimate torque, cracking patterns, failure modes, and ductility of specimens. Numerical results were in reasonable agreement with the corresponding experimental data in terms of ultimate angle of twist per unit length and ultimate torque.

Investigations on the size effect in torsional behavior of RC beams have been indicated that a size effect present (Bažant and

Şener, 1987; Bažant et al., 1988). Bažant and Şener (1987) examined the torsional failure of reinforced and unreinforced beams with rectangular cross-sections. This study assessed the applicability of a size effect law rooted in fracture mechanics principles to explain torsional failures in concrete beams without stirrups. The research confirmed the presence of a size effect; however, the exact characteristics of this effect remained uncertain due to the limitations of the available data, which were both limited and scattered. To address this issue, the study proposed a straightforward formula to account for the size effect in the analysis of such concrete beam failures. Donmez and Bažant (2017) investigated the size effect on Punching Strength of Reinforced Concrete Slabs with and without shear reinforcement. They developed a design equation for punching shear strength (v_c) by analyzing the ACI 445 database, consisting of 440 tests, and using FE modeling with the micro plane model M7. The study confirmed a size effect, with the log-log relationship between v_c and slab depth (d) being slightly milder than -1/2 within the practical size range, aligning with ACI Committee 446's endorsed energetic size effect factor. They derived and validated the design equation, adjusting for data density variations, and confirmed the size effect factor's validity through FE analysis with broader-range data. In another study by Kirane et al. (2016), the authors investigated the size effect on the torsional strength of concrete beams, including those with and without stirrups. Their findings challenged conventional assumptions, revealing that stirrups did not eliminate the size effect. They classified the size effect as Type I, indicating failure at macrocrack initiation, not after stable crack growth. This behavior was deterministic within the practical size range, contrary to earlier expectations. Calibration of their simulations with various tests validated their conclusions, demonstrating strong alignment between predictions and experimental results, including crack patterns.

Alabdulhady and Sneed (2019) conducted a review on numerical and analytical methods developed to predict the torsional behavior of FRP strengthened RC beams. Types of composites, dimensions of beam, wrapping method, mechanical characteristics of the RC beams, and modes of failure were the main parameters to investigate in that study.

While there have been numerous studies examining the torsional behavior of RC beams, it's important to note that the size effect in strengthened RC beams has not been explored in any prior research. This paper aims to address this gap by investigating the presence of a size effect on the torsional behavior of RC beams, considering different ratios of reinforcement, including both FRP sheets and steel rebars. Another key objective of this study is to conduct a parametric analysis, exploring various reinforcement ratios and different FRP strengthening methods to assess the torsional behavior of beams with four distinct cross-sections. To attain these objectives, Finite Element (FE) software, specifically ABAQUS, was utilized to construct a model capable of forecasting the torsional behavior exhibited by RC beams reinforced with FRP. The analysis encompasses an investigation into the influences of size, reinforcement ratio, and the number of FRP layers on the torsional deformation characteristics of the beams. To validate the numerical simulations, a comparative assessment was conducted against experimental data available in the academic literature.

2. Considered Experimental Study and Modeling Verification

Chalioris (2008) conducted an experimental study on 3 different groups of concrete beams. Rectangular cross-section with dimensions b_w/h = 100/200 mm and b_w/h = 150/300 mm and T-shape cross-section with dimensions $b_w/h/b_f/h_f$ = 150/300/300/50 mm was the three different beams cast in that experimental program. The behavior of 14 beams (including three control specimens without any transverse bars or FRP strengthening, eight FRP strengthened beams, and three beams with transverse reinforcement) was examined under pure torsion. Beam's length was 1,600 mm and 300 mm of that at each end was highly reinforced and fully confined to resist without cracking under applied torsional load. Diagonally placed steel spreader beam on the ends of two steel arms was used to apply the torsional loading. Fig. 1 indicates the test setup in the Chalioris study.

Two control specimens (Ra-c and Rb-c), a transverse reinforced specimen (Ra-s5.5/150), and two FRP strengthened specimens (Rb-F(1) and Rb-Fs200(1)) were taken from that study for comparison purposes and model validation. Fig. 2 shows the geometrical details of considered specimens. A comparison has been made in Fig. 3 between experimental data and numerical results obtained from this study. Torque-twist curves gained from experimental and modeling were in good agreement and as it is shown in Fig. 3 modeling was able to predict the peak torque values with good accuracy. Table 1 presents the accuracy of the validation model, revealing that the results exhibit variations within a 10% range, with a majority demonstrating high accuracy. Furthermore, Figs. 4 and 5 visually depict the cracked regions observed in the experimental study and provide comparisons with the vulnerable regions of the beam models in the numerical study, specifically focusing on fully wrapped beams and non-

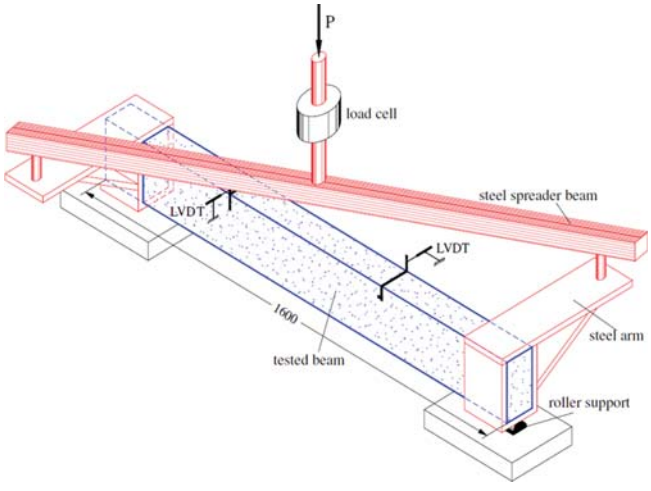

Fig. 1. Test Setup in Experimental Program (Chalioris, 2008)

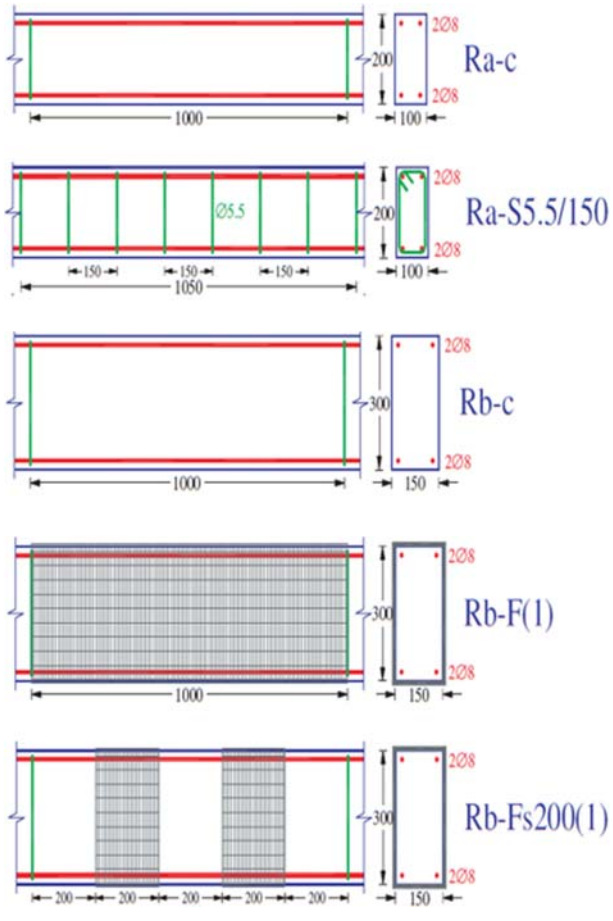

Fig. 2. Detailing of Tested Specimens (Chalioris, 2008)

strengthened RC beams, respectively. In fully wrapped beams, cracking predominantly occurs at the edges of the strengthened area, accompanied by a diagonal pattern in the central portion of the beam. In contrast, non-strengthened beams exhibit cracking in the central part of the beam, forming a diagonal pattern. It's worth noting that variations in the cracked area between Figs. 5(b) and 5(c) can be attributed to differences in transverse reinforcement and loading conditions across the two distinct studies.

3. Non-Linear FE Modeling

One of the most important parts of FE modeling is defining the nonlinear behavior of materials. To have accurate results plastic damage in concrete, yielding in steel, and damage in fiber and matrix of FRP should be carefully defined in software. Also, defining boundary conditions and contacts between different parts of the model could have a huge impact on output results. Although simplified assumptions in modeling will decrease the accuracy of the results it would be necessary to reduce the computational time cost. The assumption made in modeling will be discussed in the following section.

A total number of 24 models were used to investigate the effect of size, reinforcement ratio and number of FRP plies in the torsional behavior of RC beams. Information of models is listed in Table 2. As it is shown in Fig. 4, models have been categorized into 4 groups by their cross-section dimensions. b_w(mm)/h(mm) for groups 1 to 4 are 75/180, 150/360, 300/720, and 600/1440, respectively. Models in each group consist of 2 different reinforcement ratios and 4 different numbers of FRP plies (0, 1,

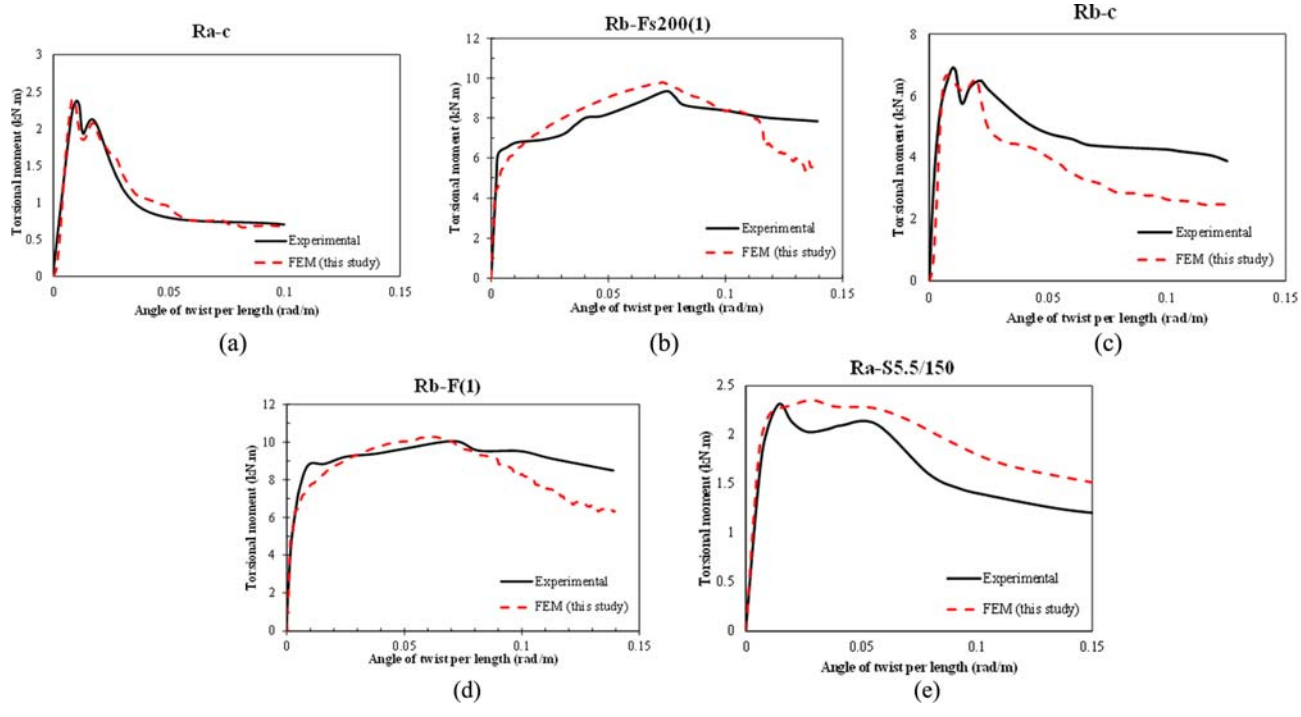

Fig. 3. Comparison of Torque-Twist Behavior in Beams: Finite Element Method (FEM) Results (this study) versus Experimental Data (Chalioris, 2008): (a) Ra-c, (b) Rb-Fs200(1), (c) Rb-c d. Rb-F(1), (e) Ra-S5.5/150

Table 1. Comparison between the Validation Models and Experimental Study

	This study	Chalioris, 2008		This study	Chalioris, 2008	
Model	T_{cr} (kN·m)	T_{cr} (kN·m)	Error (%)	T_{max} (kN·m)	T_{max} (kN·m)	Error (%)
Ra-c	2.39	2.389	0.04	2.39	2.389	0.04
Rb-Fs200(1)	6.24	6.728	7.25	9.81	9.315	5.31
Rb-c	7.17	7.36	2.58	7.17	7.36	2.58
Rb-F(1)	7.96	8.77	9.23	10.31	10.27	0.39
Ra-S5.5/150	2.22	2.3	3.48	2.22	2.3	3.48

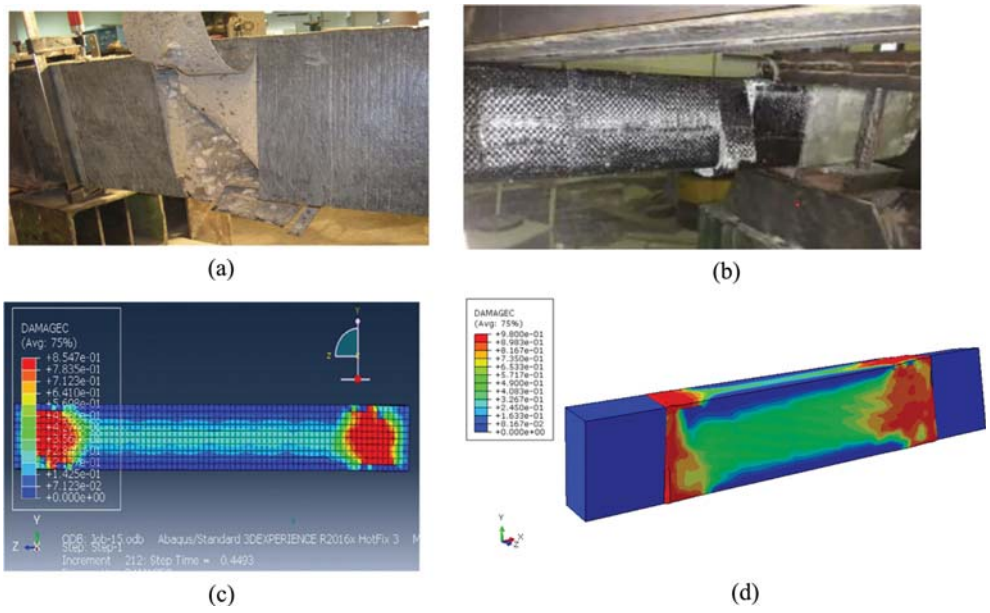

Fig. 4. Cracking Patterns Observed in Various Studies for Fully Wrapped Rectangular Beams: (a) Chalioris (experimental), (b) Mirzaie and Tavakkolizadeh (experimental), (c) Majed et al., 2021 (numerical), (d) This Study (numerical))

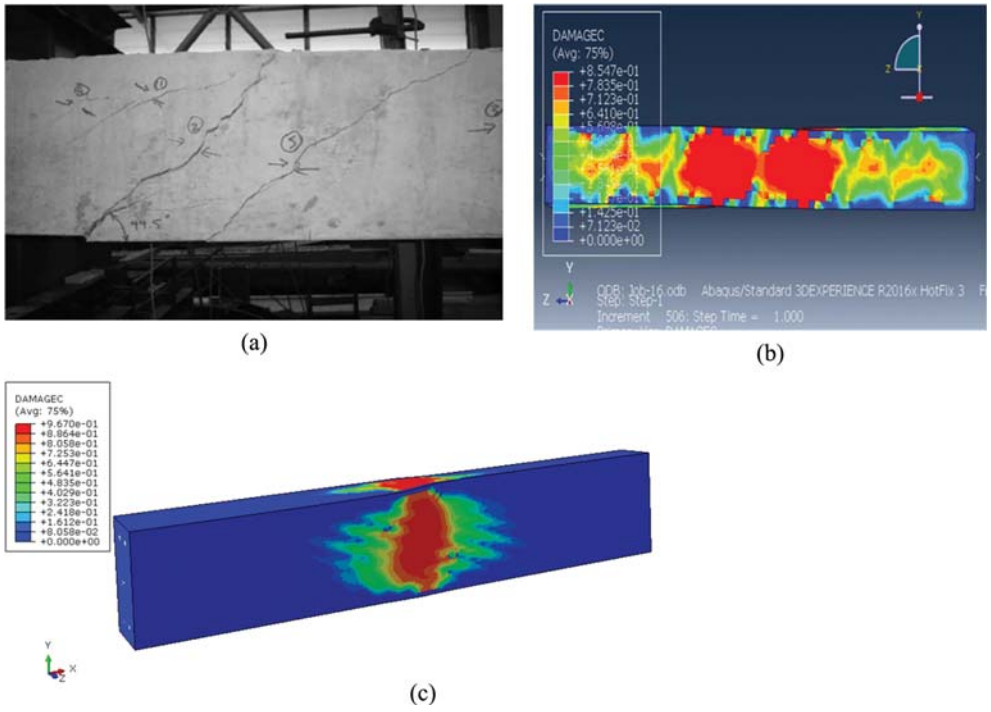

Fig. 5. Cracking Patterns Observed in Various Studies for Rectangular Beams without Strengthening: (a) Ameli (experimental), (b) Majed et al., 2021 (numerical), (c) This Study (numerical))

Table 2. Details of the Specimens

Model name	$B \times D$ (mm)	Longitudinal reinforcement (ϕ in mm)	Torsional longitudinal reinforcement (ϕ in mm)	Transverse reinforcement (ϕ in mm)	ρ_l (%)	ρ_t (%)	FRP strengthening	n_f	ρf_t (%)
1-A-RC	75 × 180	2Ø6 (Grace, Jensen et al.) - 2Ø8 (BOT)	-	Ø4@120	1.16	0.28	NO	-	-
1-A-FRP	75 × 180	2Ø6 (Grace, Jensen et al.) - 2Ø8 (BOT)	-	Ø4@120	1.16	0.28	Fully wrapped	1	0.42
1-A-FRPx2	75 × 180	2Ø6 (Grace, Jensen et al.) - 2Ø8 (BOT)	-	Ø4@120	1.16	0.28	Fully wrapped	2	0.83
1-A-FRPx3	75 × 180	2Ø6 (Grace, Jensen et al.) - 2Ø8 (BOT)	-	Ø4@120	1.16	0.28	Fully wrapped	3	1.25
1-B-RC	75 × 180	2Ø8 (Grace, Jensen et al.) - 2Ø10 (BOT)	-	Ø4@120	1.91	0.28	NO	-	-
1-B-FRP	75 × 180	2Ø8 (Grace, Jensen et al.) - 2Ø10 (BOT)	-	Ø4@120	1.91	0.28	Fully wrapped	1	0.42
2-A-RC	150 × 360	2Ø14 (Grace, Jensen et al.) - 2Ø16 (BOT)	-	Ø6@135	1.31	0.28	NO	-	-
2-A-FRP	150 × 360	2Ø14 (Grace, Jensen et al.) - 2Ø16 (BOT)	-	Ø6@135	1.31	0.28	Fully wrapped	1	0.21
2-A-FRPx2	150 × 360	2Ø14 (Grace, Jensen et al.) - 2Ø16 (BOT)	-	Ø6@135	1.31	0.28	Fully wrapped	2	0.42
2-A-FRPx3	150 × 360	2Ø14 (Grace, Jensen et al.) - 2Ø16 (BOT)	-	Ø6@135	1.31	0.28	Fully wrapped	3	0.62
2-B-RC	150 × 360	2Ø18 (Grace, Jensen et al.) - 2Ø20 (BOT)	-	Ø6@135	2.10	0.28	NO	-	-
2-B-FRP	150 × 360	2Ø18 (Grace, Jensen et al.) - 2Ø20 (BOT)	-	Ø6@135	2.10	0.28	Fully wrapped	1	0.21
3-A-RC	300 × 720	4Ø20 (Grace, Jensen et al.) - 4Ø22 (BOT)	2 × 1Ø16	Ø8@240	1.47	0.14	NO	-	-
3-A-FRP	300 × 720	4Ø20 (Grace, Jensen et al.) - 4Ø22 (BOT)	2 × 1Ø16	Ø8@240	1.47	0.14	Fully wrapped	1	0.10
3-A-FRPx2	300 × 720	4Ø20 (Grace, Jensen et al.) - 4Ø22 (BOT)	2 × 1Ø16	Ø8@240	1.47	0.14	Fully wrapped	2	0.21
3-A-FRPx3	300 × 720	4Ø20 (Grace, Jensen et al.) - 4Ø22 (BOT)	2 × 1Ø16	Ø8@240	1.47	0.14	Fully wrapped	3	0.31
3-B-RC	300 × 720	4Ø25 (Grace, Jensen et al.) - 4Ø28 (BOT)	2 × 1Ø16	Ø8@240	2.23	0.14	NO	-	-
3-B-FRP	300 × 720	4Ø25 (Grace, Jensen et al.) - 4Ø28 (BOT)	2 × 1Ø16	Ø8@240	2.23	0.14	Fully wrapped	1	0.10
4-A-RC	600 × 1440	6Ø32 (Grace, Jensen et al.) - 6Ø36 (BOT)	2 × 5Ø16	Ø10@240	1.31	0.11	NO	-	-
4-A-FRP	600 × 1440	6Ø32 (Grace, Jensen et al.) - 6Ø36 (BOT)	2 × 5Ø16	Ø10@240	1.31	0.11	Fully wrapped	1	0.05
4-A-FRPx2	600 × 1440	6Ø32 (Grace, Jensen et al.) - 6Ø36 (BOT)	2 × 5Ø16	Ø10@240	1.31	0.11	Fully wrapped	2	0.10
4-A-FRPx3	600 × 1440	6Ø32 (Grace, Jensen et al.) - 6Ø36 (BOT)	2 × 5Ø16	Ø10@240	1.31	0.11	Fully wrapped	3	0.16
4-B-RC	600 × 1440	10Ø32 (Grace, Jensen et al.) - 10Ø36 (BOT)	2 × 5Ø16	Ø10@240	2.15	0.11	NO	-	-
4-B-FRP	600 × 1440	10Ø32 (Grace, Jensen et al.) - 10Ø36 (BOT)	2 × 5Ø16	Ø10@240	2.15	0.11	Fully wrapped	1	0.05

2 and 3). The model's name consists of three parts. The first part refers to the section groups which are numbered from 1 to 4. The second part refers to the reinforcement ratio. Lower and higher reinforcement ratios are considered as group A and B, respectively. The third part indicates FRP strengthening and the number of FRP plies. It is noted that the reinforcement ratios are reported in Table 1. These values have been calculated from Eqs. (1) to (3):

$$\rho_l = \frac{A_{sl}}{A_c}, \tag{1}$$

$$\rho_t = \frac{A_{st}}{B \times s}, \tag{2}$$

$$\rho_{ft} = \frac{nf \cdot tf \cdot pf}{A_c} \cdot \frac{w_f}{sf}, \tag{3}$$

where ρ_l is longitudinal reinforcement ratio; A_{sl} is total area of longitudinal (including torsional) rebars; A_c is gross area of beam cross-section; ρ_t is transverse reinforcement ratio; A_{st} is total area of stirrups legs, B is beam width; s is stirrups spacing; ρ_{ft} is ratio of externally epoxy-bonded carbon FRP fabrics as transverse reinforcement; n_f is number of FRP plies; t_f is one FRP ply thickness; p_f is perimeter of FRP ply; w_f is width of the FRP strips; and s_f is length along the beam over that FRP area is

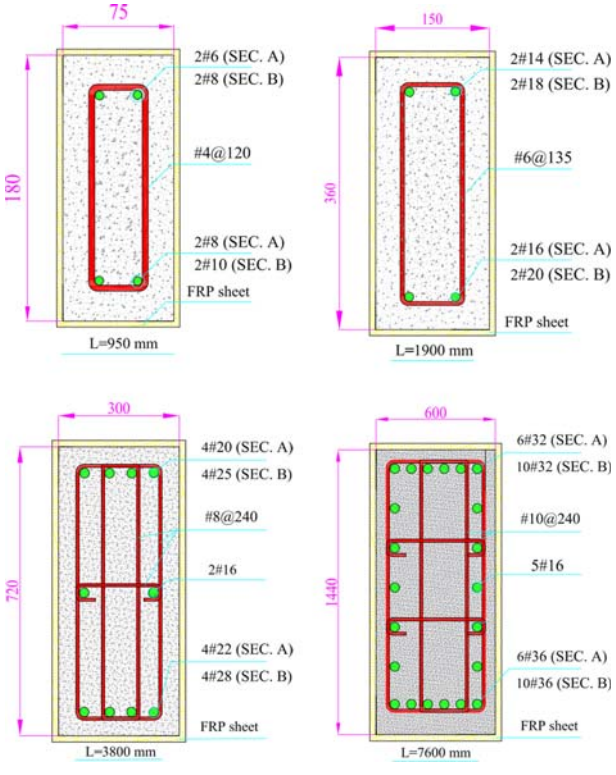

Fig. 6. Details of Cross-Sections

distributed (fully wrapped beams: $\frac{w_f}{s_f} = 1$) cross-sections of groups 1 to 4 are shown in Fig. 6.

3.1 Modeling Description

ABAQUS dynamic explicit scheme was used to model the torsional behavior of FRP strengthened RC beams. Generally, explicit analysis and integration techniques are good at modeling the nonlinear behavior of materials and convergence (Zimmermann, 2001). A condition should be considered while using dynamic explicit step in ABAQUS for a quasi-static problem and that is the ratio of kinetic energy to internal energy should be less than 10% so that the choice of using dynamic explicit step is a correct choice (Smith, 2009). The ratio of kinetic energy to internal energy was small in all models. Fig. 7 shows the assembly model and the boundary condition applied to the beam edges. It should be noted that the red areas in Fig. 7(b) are considered as rigid body. In Chalioris's study, the ends of beams were highly reinforced and confined with FRP so in modeling both ends of the beam were considered to be rigid. A displacement control scheme was used to apply the torsion on the beam. Perfect bond or cohesive modeling can be used to simulate the interaction between the FRP sheet and concrete beam. Using the perfect bonding method will lead to less computational time cost compared to the cohesive method, as well as properly accurate results (Obaidat et al., 2010). 'Tie' constraint was used to simulate the perfectly bond interaction between FRP and concrete. The effect of bond-slip between steel and concrete can be neglectable. This issue was investigated by Mondal and Prakash (Mondal and Prakash, 2016) in a study of RC beam under torsion. 'Embedded region' constrain was used to simulate the interaction between concrete and steel. flowchart of nonlinear modeling is presented in Fig. 8.

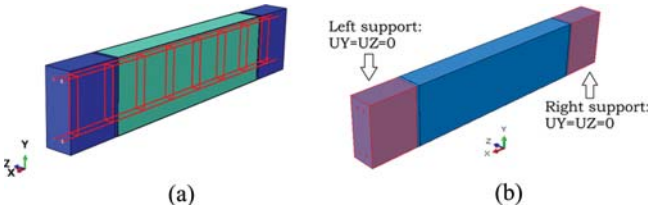

Fig. 7. Numerical Model: (a) Assembly Model, (b) Boundary Condition

3.2 Materials Idealization and Modeling

3.2.1 Concrete

Carefully definition of concrete material is very important and will have a huge impact on the results. The stress-strain curve of concrete in tension or compression consists of two branches, elastic and inelastic. The elastic behavior of concrete is defined using Young's modulus and Poisson's ratio. Nonlinear behavior is defined using the concrete damage plasticity (CDP) option in the software. The compressive strain-stress curve was defined by a parabolic model shown in Fig. 9. To develop this model in software users should input compressive stresses (σ_c) and damage parameters (d_c) for corresponding inelastic strain ($\tilde{\varepsilon}_c^{in}$) values as well as young's modulus (E_0). Inelastic strains can be calculated from Eqs. (4) and (5):

$$\tilde{\varepsilon}_c^{in} = \varepsilon_c - \varepsilon_{oc}^{el}, \tag{4}$$

$$\varepsilon_{oc}^{el} = \frac{\sigma c}{E_0}, \tag{5}$$

where ε_c is the total compressive strain and ε_{ot}^{el} is the elastic strain corresponding to the undamaged material.

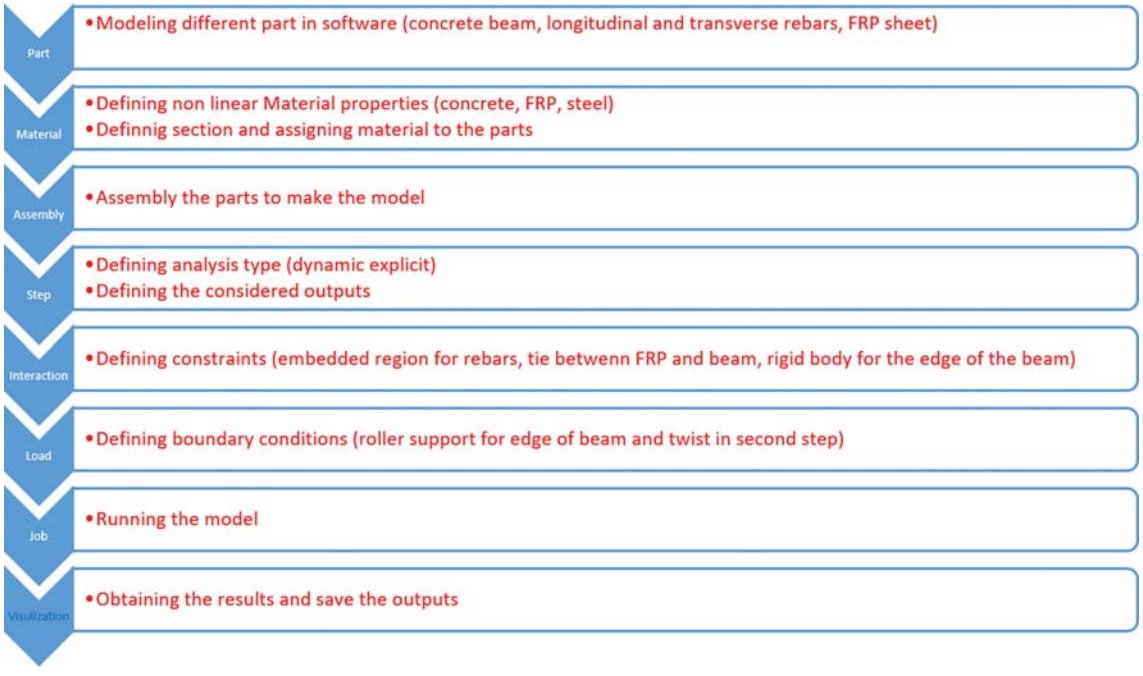

Fig. 8. Flowchart of Nonlinear Modeling

Before cracking, concrete behaves elastically, and thereafter the behavior is softened. The exponential model proposed by Greene (Greene Jr, 2006) is shown in Fig. 10 and used to model post-cracking behavior in tension. To develop this model in software users should input the tensile stresses (σ_t) and damage parameters (d_t) for corresponding cracking strain ($\tilde{\varepsilon}_t^{ck}$) values as well as Young's modulus (E_0). The cracking strain can be calculated from Eqs. (6) and (7) below:

$$\tilde{\varepsilon}_t^{ck} = \varepsilon_t - \varepsilon_{ot}^{el}, \tag{6}$$

$$\varepsilon_{ot}^{el} = \frac{\sigma_t}{E_0}, \tag{7}$$

where ε_t is the total tensile strain and ε_{ot}^{el} is the elastic strain corresponding to the undamaged material.

Other than compressive and tensile behavior, plasticity should be defined in the CDP option by 5 items, including dilation angle (Ψ), flow potential eccentricity (e), viscosity (μ), biaxial to uniaxial strength ratio ($\frac{f_{bo}}{f_{co}}$), and tensile to compressive meridian stress ratio (K). CDP input values are listed in Table 3. The values are obtained from the literature (Yu et al., 2010; Lee et al., 2020) and calibrated by experimental results. The compressive and tensile behavior of concrete are also presented in Table 3 in terms of yield stress and inelastic strain.

C3D8R elements are used to model the concrete. This is an 8-

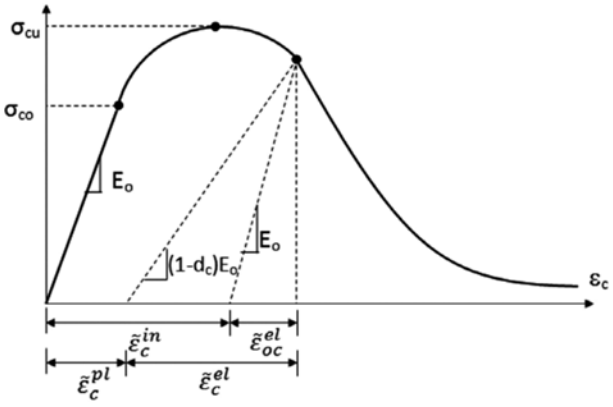

Fig. 9. Elastic and Inelastic Behavior of Concrete in Compression (Demin and Fukang, 2017)

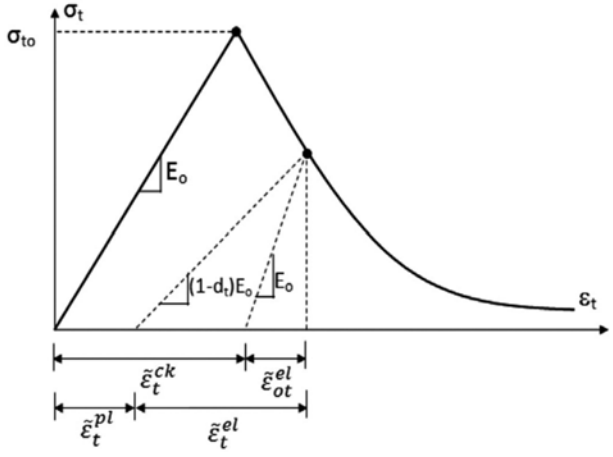

Fig. 10. Elastic and Inelastic Behavior of Concrete in Tension (Wahalathantri et al., 2011)

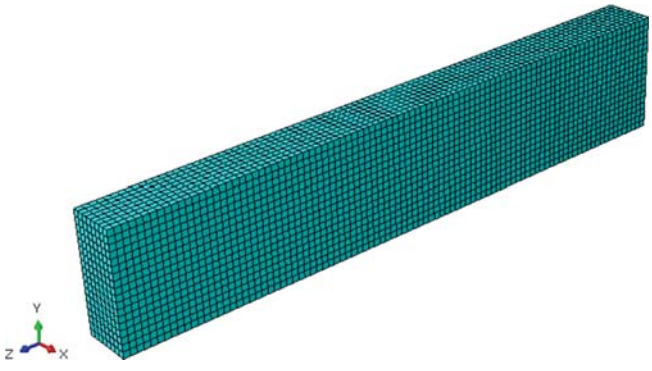

Fig. 11. Meshing of Concrete Beam

Table 3. Concrete Properties in ABAQUS

Density (kg/m^3)	Elastic modulus (GPs)	Poison's ratio	Dilation Angle (ψ)	Eccentricity (e)	Viscosity (μ)	f_{b0}/f_{c0}	K	Compressive Strength (MPa)	Tensile Strength (MPa)
2,400	14.5	0.15	37	0.1	0.001	1.16	0.67	27.5	2.9
Compressive behavior					Tensile behavior				
Yield stress (Pa)		Inelastic strain			Yield stress (Pa)			Cracking strain	
10500000		0							
20681175.12		7E-05							
28817268.79		0.00071							
27429131.56		0.00181							
22493409.97		0.003							
18203172.87		0.00417			3000000			0	
13599680.25		0.00585			300000			0.018	
9208977.375		0.00845							
5656174.453		0.01266							
2356145.628		0.02487							
929960.201		0.04994							
494520.4276		0.07996							

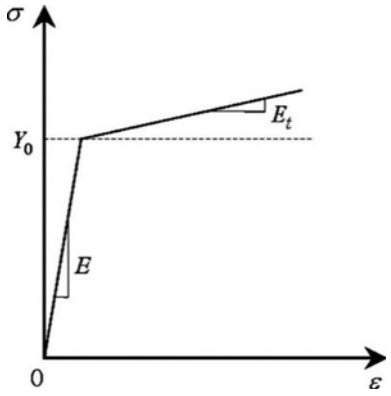

Fig. 12. Elastic and Inelastic Behavior of steel (Sæther and Sand, 2012)

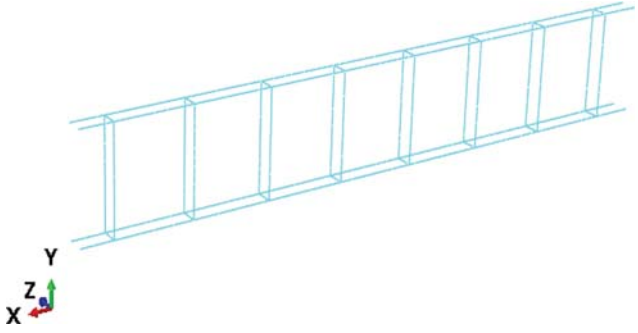

Fig. 13. Meshed Steel Rebar

node solid brick element with three translational degrees of freedom at each node which has the capability of cracking in three orthogonal directions, plastic deformation and crushing. The concrete part meshed with a general size of 10 mm has shown in Fig. 11.

3.2.2 Steel

Elastic modulus and Poisson's ratio were used to define the elastic behavior of steel. Perfectly plastic behavior is defined by using inelastic strain and corresponding yield stress. Fig. 12 indicates the stress-strain relationship of steel material in both elastic and plastic zone.

For elastic behavior of steel, elastic modulus was defined 210 GPa with a Poisson's ratio of 0.3 and for plastic behavior yield stresses, 560 MPa and 760 MPa were defined for the corresponding 0 and 0.2 plastic strains. 2-node linear three-dimensional (T3D2) was used to model steel longitudinal and transverse bars. Fig. 13 shows the meshed longitudinal and transverse rebars. The meshing was applied by a seed size of 5 mm.

3.2.3 FRP

The tensile behavior of FRP material was considered to be elastic and strain will increase linearly until the tensile strength. Fig. 14 indicates a simple bilinear traction–separation law in FRP.

Hashin damage criteria were used to simulate the damage in FRP. The thickness of FRP fabric was 0.11 mm. The mechanical properties of FRP are reported in Table 4.

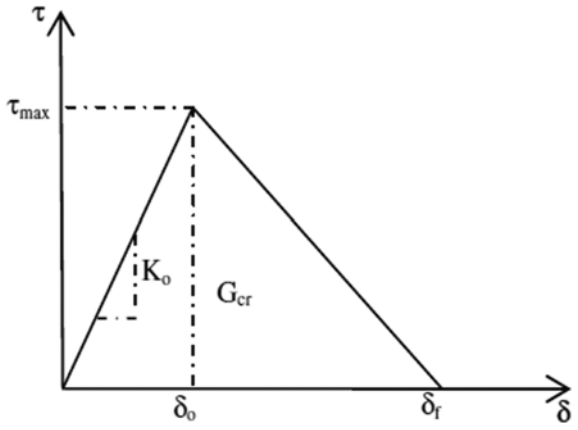

Fig. 14. Traction–Separation Law in FRP (Mohammadi et al., 2013)

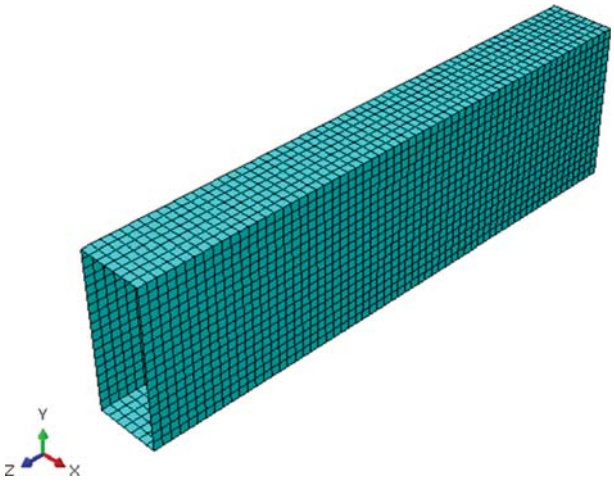

Fig. 15. Meshed FRP Fabric

Table 4. FRP Mechanical Properties (Prakash et al., 2016)

Elastic modulus (GPs)	E1	60.80
	E2	58.25
	E3	58.25
Poison's ratio	μ_{12}	0.07
	μ_{31}	0.07
	μ_{23}	0.4
Shear modulus (GPs)	G_{12}	4.55
	G_{31}	4.55
	G_{23}	5
Shear strength (MPa)	S_{12}	125
	S_{23}	125
Compressive strength (MPa)	X_C	760
	Y_C	707
Tensile strength (MPa)	X_T	621
	Y_T	594
Density (kg/m^3)	ρ	1,560
In plane fracture toughness (kJ/m^2)	$G_{1C}{}^T$	160
	$G_{2C}{}^T$	10
	$G_{1C}{}^C$	25
	$G_{2C}{}^C$	2.25

A 4-node doubly curved shell with reduced integration and hourglass control (S4R) elements were used to model the FRP. FRP sheet with an element size of 10 mm is shown in Fig. 15.

4. Result and Discussion

4.1 Damage in Materials

Results for the model 1-A-FRP are presented in this section as an example for investigation damage in FRP, concrete, and rebars. Similar results were observed for all other specimens.

Hashin damage criteria were used for modeling damage in the FRP sheet. When the magnitude of this criteria reaches 1 it means that damage has occurred. Fig. 16 shows the damage in tension and compression for both matrix and fiber of FRP. As it is clear main damage was for the matrix in tension, after 0.03 radian of rotation, FRP damage starts to take place and spread until 0.1 radians. At 0.1 radians some elements at the middle part of FRP were deleted due to rupture in FRP.

Figure 17 illustrates the equivalent plastic strains (PEEQ) which represent the onset of concrete inelasticity or cracking. These PEEQ values become non-zero, signaling the initiation of plastic strain. Notably, plastic strain commences in the central portion of the beam after the application of load.

Equivalent compressive and tensile plastic strains equal to 0.0379 and 0.0106 at 0.1 radian.

For investigating steel behavior in RC beam, Von Mises stress was used to predict yielding in steel. As yielding stress was defined 560 MPa, so when Von Mises stress reaches this value steel starts to yield. Yielding in steel starts to take place at 0.094 radians in middle transverse rebars. Maximum Von Mises stress at 0.1 radians was 514 MPa for longitudinal rebars and 560.3 MPa for transverse rebars. It means that longitudinal rebars remain at their elastic range while transverse rebars have plastic deformation.

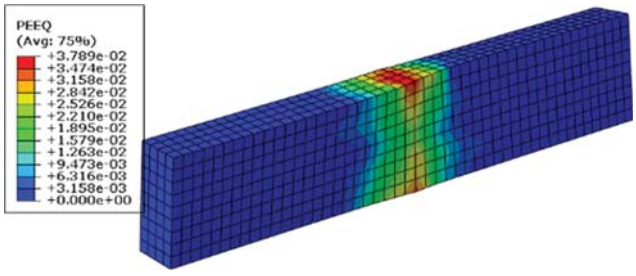

Fig. 17. Equivalent Plastic Strain in Concrete

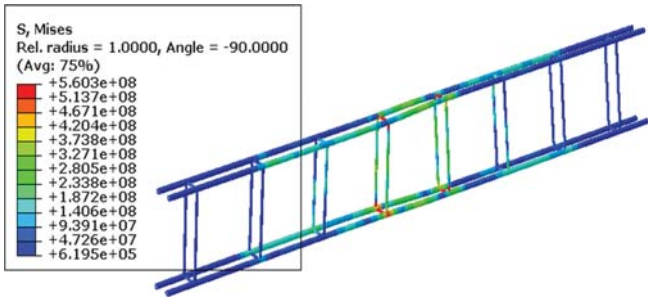

Fig. 18. Von Mises Stress in Rebars at 0.1 Radian

Fig. 18 indicates the Von Mises stress in rebars at 0.1 radians.

4.2 Torsional Strength and Torque-Twist Response

The measured cracking torsional moments (T_{cr}), corresponding angle of twist per length (ϑ_{cr}), the post-cracking ultimate torsional moments (Hussain Q), and corresponding angle of twist per unit length (ϑ_{Tu}), and the peak torque (T_{max}) values are presented in Table 5. Also, Fig. 16 presents the torque-twist behavior of models of groups 1 to 4. For 16 beams T_{max} was equal to T_{cr} as they didn't demonstrate further increase in the torsional moment after cracking. A similar behavioral pattern was seen in the

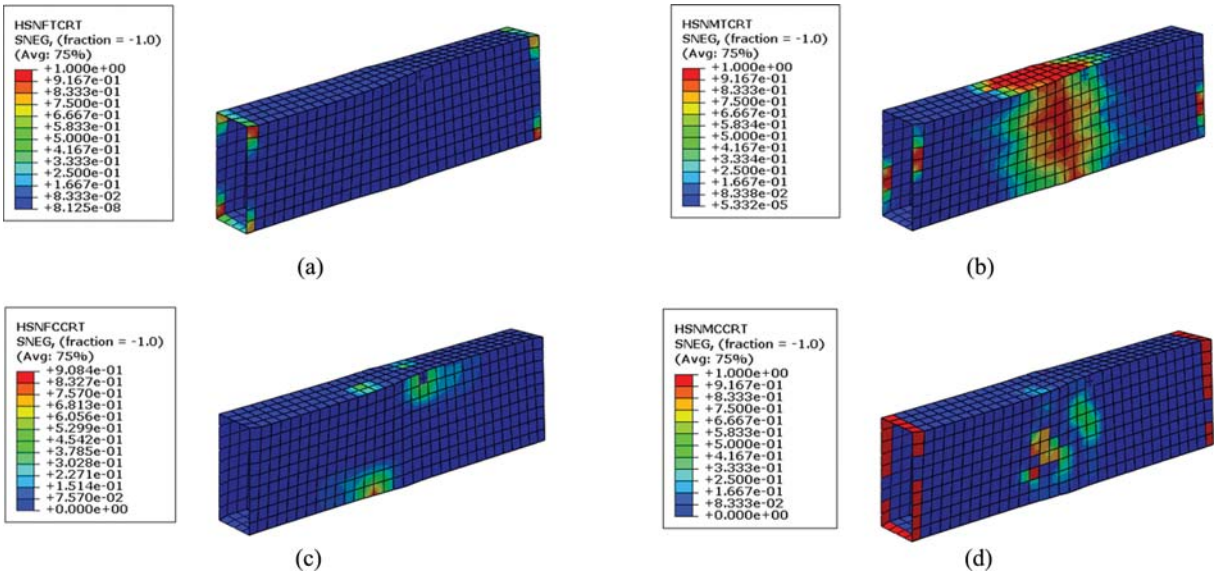

Fig. 16. Damage in FRP at 0.1 Radian: (a) Damage in Fiber in Tension, (b) Damage in the Matrix in Tension, (c) Damage in Fiber in Compression, (d) Damage in the Matrix in Compression

beams Ra-a, Rb-c, Ra-S5.5/150, Rb-S5.5/160, Tc, and T-FU(1) in the Chalioris (Chalioris, 2008) study. For the other 8 beams, T_{max} was equal to T_u. These eight beams exhibit post-cracking behavior, indicating the adequacy and effectiveness of steel reinforcements and/or FRP strengthening in enhancing torsional capacity. FRP sheets significantly enhance the torsional capacity of Reinforced Concrete (RC) beams through a combination of mechanisms. These include confinement, improved shear strength, increased stiffness, shear force transfer, and composite action. These mechanisms collectively mitigate torsional failure modes and boost the beam's resistance to torsion. This observation underscores the importance of these structural improvements in the context of designing for torsion resistance. Furthermore, this observed behavior aligns with the findings of the broader Chalioris study, which covers beams not specifically mentioned here. The torsional moment progression in these beams follows a distinct pattern. Initially, there is a linear increase in torsional moment until cracking occurs. Beyond this critical threshold, the material behavior becomes nonlinear. Notably, cracking consistently initiates at earlier levels of torsional deformation, typically between 0.012 and 0.018 in all examined structural models. Once peak torsional strength is achieved, there is a noticeable decrease in torsional moment. This decline indicates that the structure has reached its maximum resistance to torsional forces. Subsequently, there is no significant increase in torsional moment, signifying a fundamental structural change post-cracking. This comprehensive understanding of post-cracking behavior is crucial for assessing beam performance and guiding the design and reinforcement strategies in concrete structures subjected to torsional stresses.

Table 5. Results of Numerical Models

Model name	T_{cr}	ϑ_{cr}	T_u	ϑ_{Tu}	T_{max}
1-A-RC	1.33	0.012	-	-	1.33
1-A-FRP	1.79	0.014	1.88	0.019	1.88
1-A-FRPx2	1.79	0.012	2.03	0.134	2.03
1-A-FRPx3	1.79	0.012	2.2	0.144	2.2
1-B-RC	1.34	0.013	1.37	0.026	1.37
1-B-FRP	1.84	0.014	1.9	0.019	1.9
2-A-RC	11.5	0.015	-	-	11.5
2-A-FRP	11.8	0.013	-	-	11.8
2-A-FRPx2	13.5	0.014	14.6	0.086	14.5
2-A-FRPx3	14.2	0.011	20.6	0.144	20.6
2-B-RC	11.8	0.013	-	-	11.8
2-B-FRP	11.9	0.013	-	-	11.9
3-A-RC	111	0.016	-	-	111
3-A-FRP	115	0.015	-	-	115
3-A-FRPx2	117	0.015	-	-	117
3-A-FRPx3	119	0.018	122	0.064	122
3-B-RC	114	0.016	-	-	114
3-B-FRP	116	0.016	-	-	116
4-A-RC	789	0.014	-	-	789
4-A-FRP	806	0.014	-	-	806
4-A-FRPx2	820	0.014	-	-	820
4-A-FRPx3	826	0.014	-	-	826
4-B-RC	793	0.014	-	-	793
4-B-FRP	833	0.014	-	-	833

The theoretical torsional crack of the beam with no FRP and rebar reinforcement are calculated from Eq. (8) (ACI 318-08, 2008) and presented in Table 6.

$$Ttcr = 0.33\sqrt{f_c'}\left(\frac{A_c^2}{p_{cp}}\right), \tag{8}$$

where A_c is the total gross area of beam cross-section, f_c' is the compressive strength of concrete, and P_{cp} is the perimeter of the beam.

The presence of reinforcement causes a huge difference between the cracking torsional moments of the beams. Also, rebars causes more than 50% difference between the cracking torsional moment of the reinforced and unreinforced beams.

A correlation was established to examine the influence of fiber-reinforced polymer (FRP) on torsional behavior. Fig. 19 illustrates the impact of FRP on torsional behavior across various beam sizes. Group A beams, each of different sizes, were selected to assess how FRP influenced their torsional behavior. In this Figure, the horizontal axis represents beam size, while the vertical axis represents the ratio of the torsional maximum strength of the FRP-strengthened beam to that of a corresponding, non-strengthened beam. The results indicate that in small beams, the effect of FRP is significant, with an enhancement of approximately 40%. However, in larger beams, the impact of FRP is comparatively minimal.

4.3 Size Effect on Torsional Behavior

The values of cracking moments of the beams are presented in this section to investigate the effect of size on 4 different groups

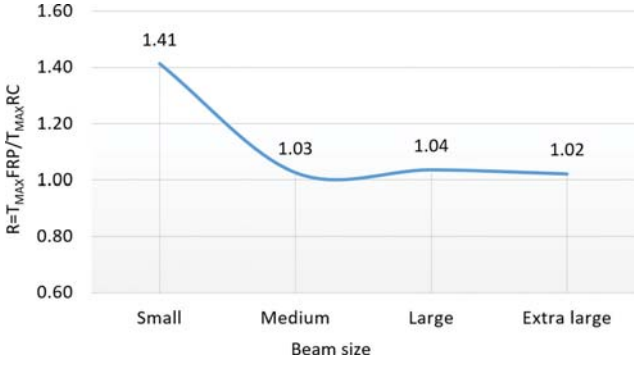

Fig. 19. The Effect of FRP in Different Beam Sizes

Table 6. The Theoretical Torsional Crack of the Beam

Beam size	B × D (mm)	T_{cr} (kN·m)
Small	75 × 180	0.624
Medium	150 × 360	5.01
Large	300 × 720	39.98
Extra large	600 × 1,440	319.82

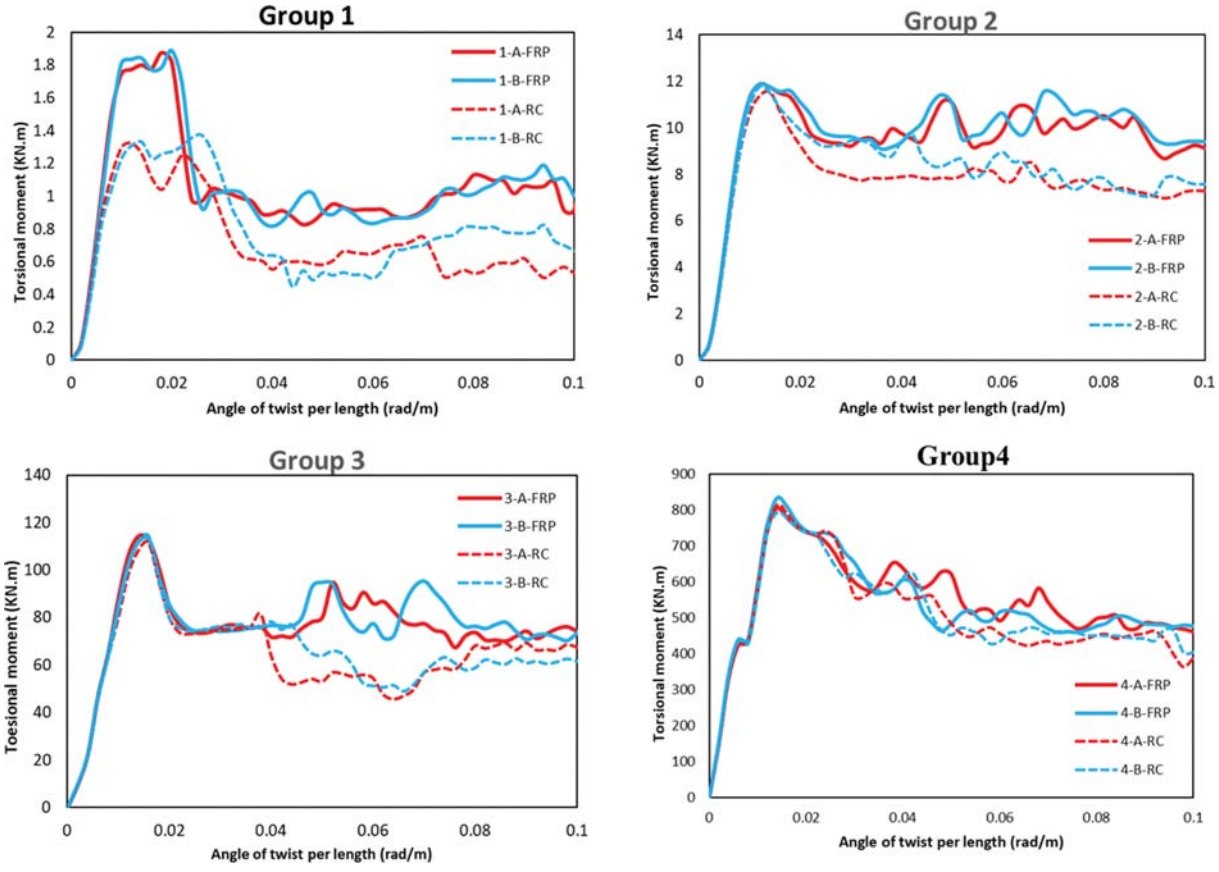

Fig. 20. Torque-Twist Curve of Beams

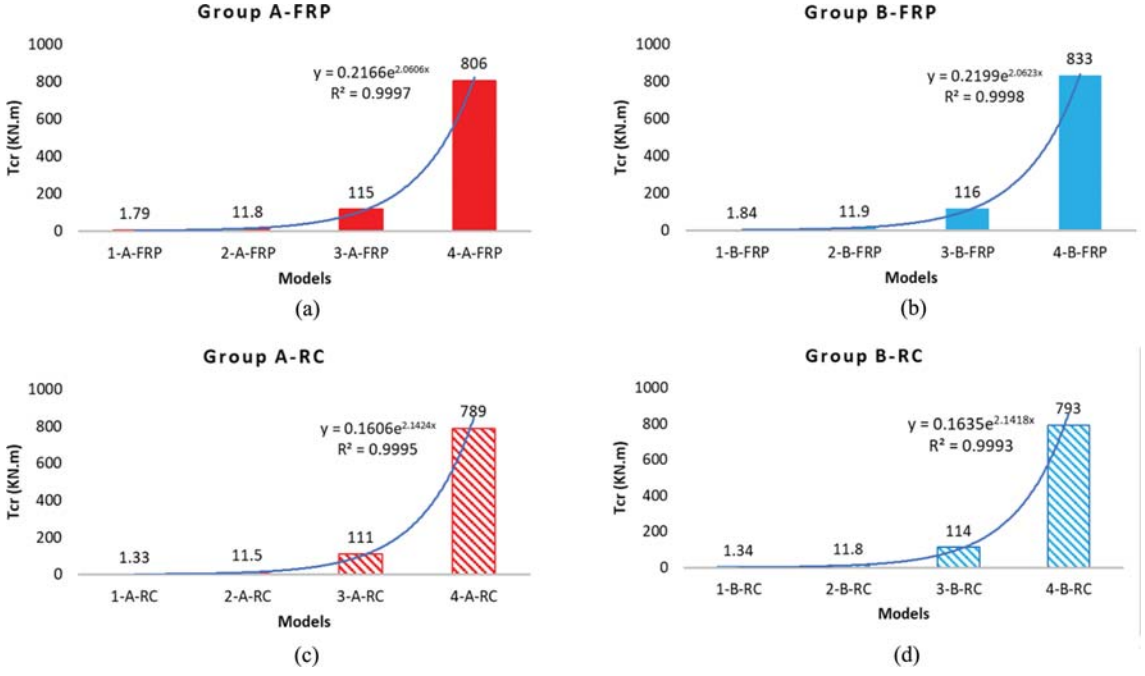

Fig. 21. Effect of Size on Cracking Moment on Different Groups: (a) Group A-FRP, (b) Group B-FRP, (c) Group A-RC, (d) Group B-RC

of specimens. The models chosen for each chart are similar in terms of the reinforcement type from groups 1 to 4. The dimensions of the cross-section are being doubled at each time.

Figure 20 presents torque-twist behavior of the models separated by types of reinforcing. The increase in the cracking moment values of FRP-confined beams with type A and B reinforcing

rebars are similar and averagely 553%, 874%, and 609% from group 1 to 2, group 2 to 3, and group 3 to 4, respectively (See Fig. 21). The same values for the RC beams (no FRP) with type A and B reinforcing rebars are 773%,866%, and 603%. Models 1-A-FRP, 2-A-FRPx2, and 3-A-FRPx3 have a close value of ratios of reinforcement, and a comparison of these models with models 1-A-RC, 2-A-RC, and 3-A-RC, shows a 34%, 17%, and 7% increase in cracking moments. It can be concluded that with the bigger values of the beam's dimension, FRP reinforcing becomes less effective. Furthermore, in group 4 beams even 3 plies of FRP do not affect the torsional strength and it may be not cost-effective to use FRP strengthening.

Based on the results obtained in this section, it can be concluded that the most effective means of increasing torsional capacity is by augmenting the dimensions of the beam, as this factor exerts a substantial influence on the beam's torsional strength. In cases where the use of larger beams is not feasible, employing FRP strengthening represents a viable alternative, particularly beneficial for small and medium-sized beams. Conversely, increasing longitudinal reinforcement is found to be an ineffective and less advantageous method for enhancing torsional capacity.

Figure 22 shows the torsional moment at 0.01 radians and 0.1 radians are defined as T_{cr0} and T_{cru}, respectively. At 0.01 radians specimens are close to cracking and at 0.1 radians they all experienced damage in steel, FRP. For comparing purposes these two angles of twist were selected as all groups have similar behavior at the mentioned stages. The ratio of $\frac{T_{cru}}{T_{cr0}}$ for effective depth (D) of beams in all groups are presented in Table 7. Also, Fig. 22 demonstrate $\frac{T_{cru}}{T_{cr0}}$ versus effective depth (D). According to results, as the effective depth increases the ratio of $\frac{T_{cru}}{T_{cr0}}$ firstly increases sharply, then increases smoothly, and finally decreases. The same pattern was seen for all groups.

Based on the theory presented in the study of the Kirane et al. (Kirane et al., 2016) the nominal torsional strength v_u for beams of rectangular cross section was defined as:

$$v_u = \frac{T_{max}}{\alpha B^2 D}, \text{ where } \alpha = \frac{1}{2}\left(1 - \frac{B}{3D}\right). \quad (9)$$

In this formula, "T_{max}" represents the peak torque, while "B" and "D" correspond to the shorter and longer sides of the rectangle, respectively. Although this is a plastic limit analysis formula, coefficient α was based on the elasticity solution.

The nominal strengths of beams of varying sizes are depicted in Fig. 23, following a similar approach to Kirane et al.'s study. This Figure illustrates the relationship between nominal torsional strength and the depth of the beam. From the graph, it is evident that in RC beams without FRP confinement, the nominal strength initially increases and then decreases with increasing depth. Conversely, in beams strengthened with FRP, the impact of FRP confinement on small-size beams with a depth of 180 mm is particularly striking. Initially, as the depth of the strengthened beam increases, the nominal strength experiences a significant reduction. Subsequently, as the influence of the FRP strengthening diminishes, the trend resembles that of the non-strengthened beams. This pattern of increase and decrease is a recurring theme

Table 7. Ratio of (T_{cru}/T_{cr0}) in All Models

Model name	$D(m,m)$	T_{cru}/T_{cr0}	T_{cr}	T_{cr0}
1-A-RC	130	0.51	1.27	0.64
2-A-RC	310	0.68	10.65	77.28
3-A-RC	670	0.73	79.71	58.54
4-A-RC	1390	0.67	577.93	387.14
1-A-FRP	130	0.52	1.75	0.91
2-A-FRP	310	0.81	11.30	9.12
3-A-FRP	670	0.84	88.17	74.00
4-A-FRP	1,390	0.78	591.89	461.49
1-B-RC	130	0.55	1.81	1.01
2-B-RC	310	0.83	11.30	9.42
3-B-RC	670	0.87	85.16	73.78
4-B-RC	1,390	0.82	582.85	477.25
1-B-FRP	130	0.54	1.23	0.67
2-B-FRP	310	0.69	10.94	7.58
3-B-FRP	670	0.75	81.65	61.56
4-B-FRP	1,390	0.71	570.74	403.82

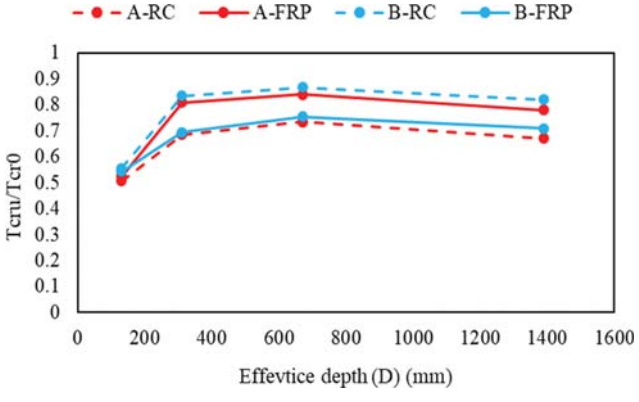

Fig. 22. Size Effect in the Torsional Behavior of Different Groups of the Beams

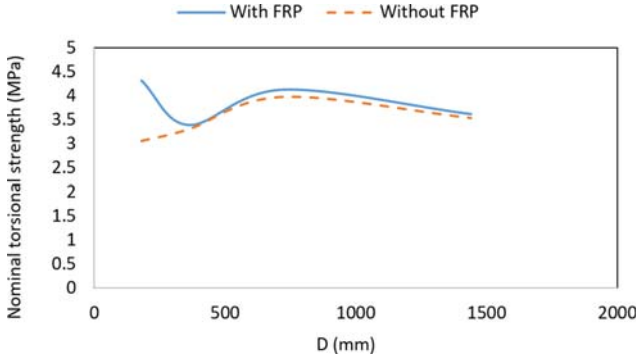

Fig. 23. The Nominal Torsional Strength of the Beams versus Beam Depth

in these beams, and we observe it when examining the ratio of $\frac{T_{cru}}{T_{cr0}}$ in Fig. 22, as well as in the nominal torsional strength illustrated in Fig. 23.

4.4 Effect of Reinforcement Ratio on Torsional Behavior

Type B steel reinforcing ratios are more than type A steel reinforcing ratios and it led to a small increase in the torsional strength of the beams. These increasement equals to 0.8%, 2.6%, 2.7%, and 0.5% for RC beams (without FRP) in group 1 to 4, respectively. Similar results were obtained in a study conducted by Zhou et al. (Zhou et al., 2017) on different groups of beams with varying longitudinal reinforcement ratios. Their findings indicated a slight increase in torsional cracking and ultimate strength with higher longitudinal reinforcement ratios.

The same values for FRP-strengthened beams are 2.8%, 0.9%, 0.9%, and 3.35%. While the influence of increasing longitudinal reinforcement ratios is not seen to be significant, the influence of FRP strengthening is so clear. After strengthening beams by FRP fabrics the average increase in cracking moments is 36%, 1.72%, 2.66%, and 3.6% for groups 1 to 4, respectively. The difference in these values is due to the difference in FRP and steel reinforcement ratios. Although there is no significant pattern in the nonlinear part of the torque-twist curves, in this region torsional moment values for beams with type B reinforcement have a bigger quantity than for beams with type A reinforcement in general. The effect of reinforcement on the cracking moment of different groups are demonstrated in Fig. 24.

4.5 Effect of Number of Plies on Torsional Behavior

The torque-twist behavior of beams with different numbers of FRP plies is presented in Fig. 25. Five beams of group 1, two beams of group 2, and a beam in group 3 have a significant increase in their torsional strength after the cracking in concrete. The adequate number of FRP ply with a thickness of 0.11 mm for having an increase in torsional strength is 1,2, and 3 for the beams of groups 1 to 3, respectively. The ratio of FRP as transverse reinforcement for these values are 0.42%, 0.42%, and 0.31%, respectively. Three layers of FRP with a thickness of 0.11 (with an FRP reinforcement ratio of 0.16%) do not affect the torsional strength of the beams of group 4. To make an influence on the torsional strength of a beam with a big cross-section high number of FRP plies may be required and strengthening the beams with a big size by FRP fabrics may be hard and not cost-effective.

The influence of the numbers of FRP plies on the cracking moment is small while it has a significant impact on the ultimate torsional strength of the beams. The ultimate torsional strength of group 1 beams is 1.88 kN·m, 2.03 kN·m, and 2.20 kN·m for 1,2, and 3 layers of strengthening, respectively. This indicates an average of 8.2% growth in ultimate strength with 0.4% increase in FRP strengthening ratio. Similar results were also observed in Chalioris's study, where the complete wrapping of RC beams with FRP sheets significantly increased the ultimate torsional strength of the beams. Additionally, Majed et al. (2021) conducted a similar investigation and concluded that their parametric study demonstrated an enhancement in torsional capacity with an increase in the number of FRP plies. In Majed et al. (2021) study, the utilization of varying numbers of plies of continuous FRP laminates wrapped around the cross-section of rectangular beams along their entire length led to a substantial increase in ultimate torsional strength, ranging between 36% and 55% compared to the control beam. The disparity in the extent of strength improvement

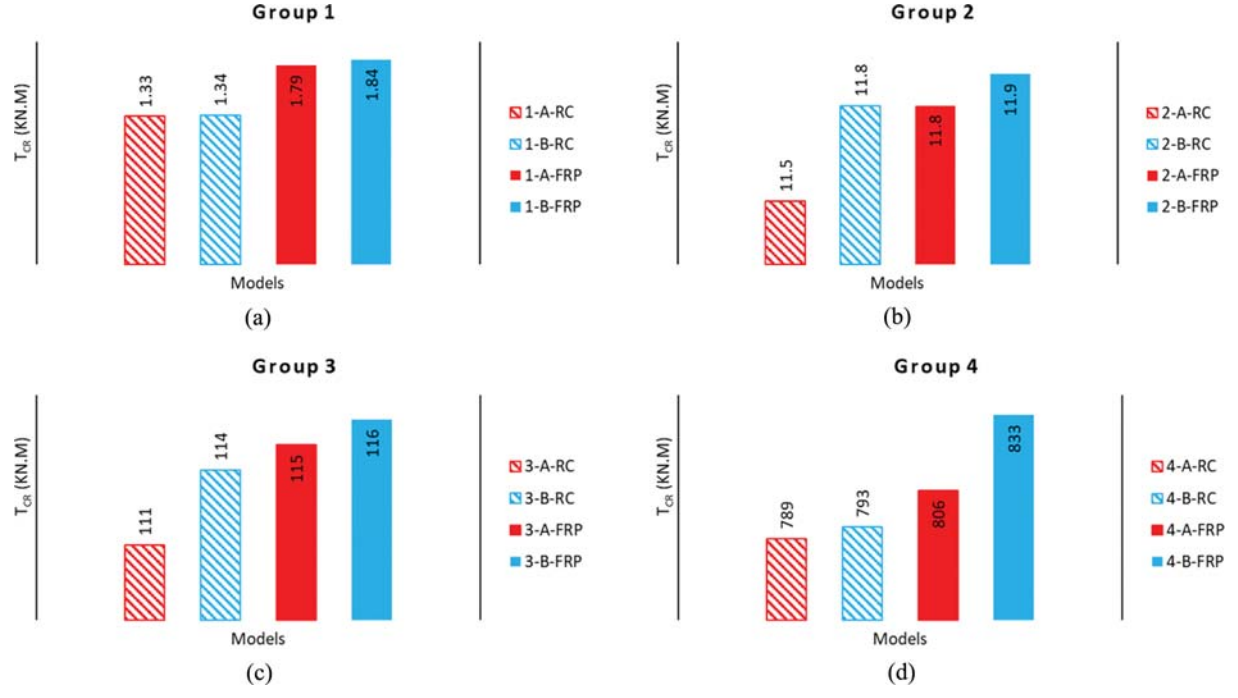

Fig. 24. Effect of Reinforcement on the Cracking Moment of Different Groups: (a) Group 1, (b) Group 2, (c) Group 3, (d) Group 4

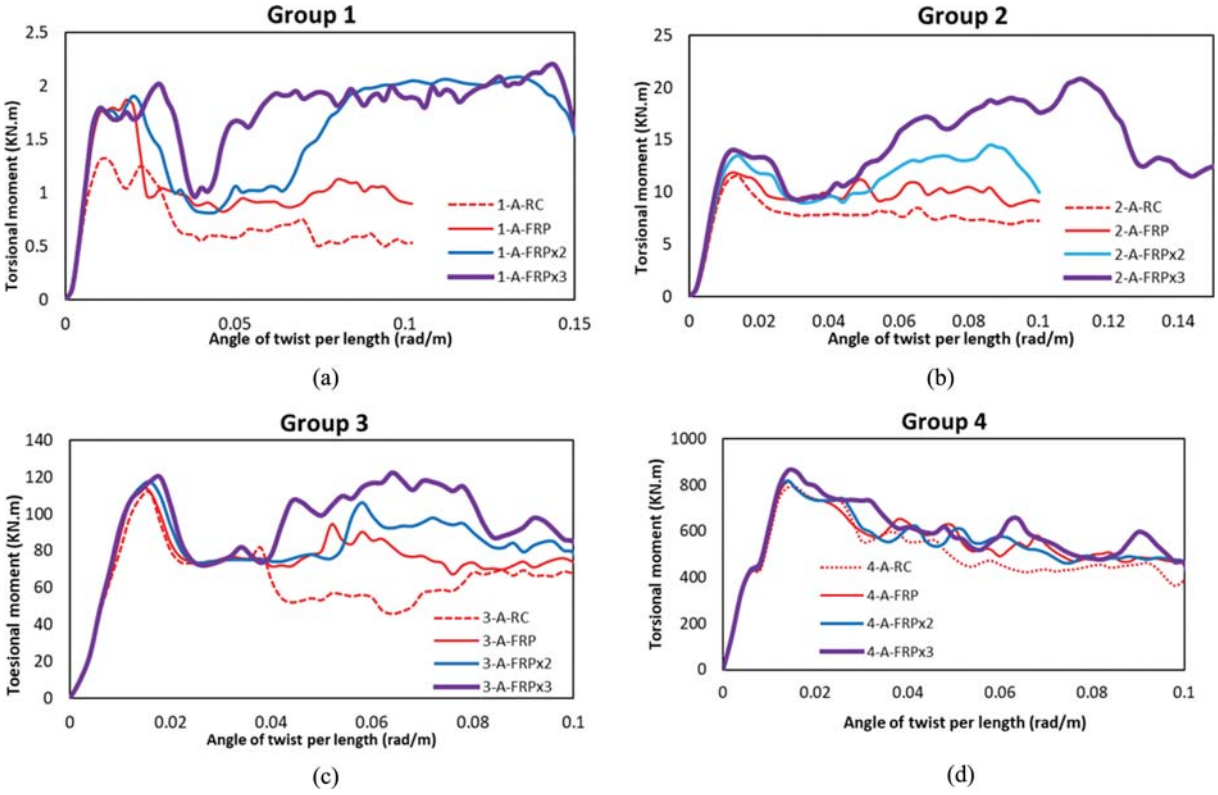

Fig. 25. Torque-Twist Behavior of Models with Different Numbers of FRP Plies in Different Groups: (a) Group 1, (b) Group 2, (c) Group 3, (d) Group 4

between Majed et al. (2021) study and the current research can be attributed to differences in FRP thickness and beam cross-section.

5. Conclusions

In this paper, the torsional behavior of FRP strengthened RC beams were numerically investigated using FE software ABAQUS. The modeling was validated with experimental data. Concrete damage plasticity, hashin damage criteria, and Von Mises stress were used to investigate the damage in concrete, FRP, and steel, respectively. The torque-twist curve, cracking torque and corresponding cracking twist, and ultimate torsional strength were evaluated for all 24 models. According to the results and observations for 4 different cross-section dimensions and 2 type of steel reinforcement and 4 type of number of FRP plies, the following conclusion can be drawn:

1. The nonlinear FE model was able to predict the torsional behavior of RC beams with and without FRP strengthening. The damages are seen in the middle of concrete material, FRP, and transverse reinforcement.
2. In 8 models with adequate steel and FRP reinforcement the ultimate torsional strength was more than cracking torsional strength. In other 16 models the maximum torsional moment was cracking moment as they did not demonstrate post-cracking behavior.
3. To investigate the size effect on the torsional behavior of FRP strengthened RC beams a relation between the effective depth of beam (D) and the ratio of the torsional moment at 0.01 to the torsional moment at 0.1 radians are presented. The results indicate a size effect on the torsional behavior of RC beams with and without strengthening. By increasing the dimensions of cross-section, the ratio of the mentioned torsional moments first increases and then decreases.
4. No considerable increase was seen in torsional strength when the longitudinal reinforcement ratio was increased by 0.1%.
5. The adequate number of FRP plies with the thickness of 0.11 mm to increase the torsional strength was 1, 2, and 3 for small beams (b/h = 75/180 mm), medium beams (b/h = 150/360 mm), large beams (b/h = 300/720 mm), respectively.
6. Even by 3 layers of FRP confinement the torsional strength of extra-large beams (b/h = 600/1440 mm) did not demonstrate any increase. Using FRP-confinement may be not practical or cost effective for extra-large beams.

Acknowledgments

Not Applicable

ORCID

Mojtaba Shokri https://orcid.org/0009-0006-7009-1085
Mahmoud Edalati https://orcid.org/0000-0002-9120-9162
S. Mohammad Mirhosseini https://orcid.org/0000-0001-7747-1132

Ehsanollah Zeighami https://orcid.org/0000-0001-9865-8019

References

ACI 318-08 (2008) Building code requirements for structural concrete (ACI 318-08) and commentary. ACI 318-08

Agarwal P, Gupta A, Angadi RG (2014) Effect of FRP wrapping on axial behavior of concrete and cyclic behavior of external RC beam column joints. *KSCE Journal of Civil Engineering* 18(2):566-573, DOI: 10.1007/s12205-014-0259-y

Akguzel U (2011) Seismic performance of FRP retrofitted exterior RC beam-column joints under varying axial and bidirectional loading. PhD Thesis, University of Canterbury, New Zealand, DOI: 10.26021/2821

Al-Rousan RZ, Issa MA (2017) Flexural behavior of RC beams externally strengthened with CFRP composites exposed to severe environment conditions. *KSCE Journal of Civil Engineering* 21(6):2300-2309, DOI: 10.1007/s12205-016-0570-x

Alabdulhady MY, Sneed LH (2019) Torsional strengthening of reinforced concrete beams with externally bonded composites: A state of the art review. *Construction and Building Materials* 205:148-163, DOI: 10.1016/j.conbuildmat.2019.01.163

Ameli M, Ronagh HR, Dux P (2007) Behavior of FRP strengthened reinforced concrete beams under torsion. *Journal of Composites for Construction* 11(2):192-200, DOI: 10.1061/(ASCE)1090-0268(2007)11:2(192)

Bakis CE, Bank LC, Brown VL, Cosenza E, Davalos JF, Lesko JJ, Machida A, Rizkalla SH, Triantafillou TC (2002) Fiber-reinforced polymer composites for construction-state-of-the-art review. *Journal of Composites for Construction* 6(2):73-87, DOI: 10.1061/(ASCE)1090-0268(2002)6:2(73)

Bažant ZP, Şener S (1987) Size effect in torsional failure of concrete beams. *Journal of Structural Engineering* 113(10):2125-2136, DOI: 10.1061/(ASCE)0733-9445(1987)113:10(2125)

Bažant ZP, Şener S, Prat PC (1988) Size effect tests of torsional failure of plain and reinforced concrete beams. *Materials and Structures* 21(6):425-430, DOI: 10.1007/BF02472322

Chalioris C (2008) Torsional strengthening of rectangular and flanged beams using carbon fibre-reinforced-polymers–Experimental study. *Construction and Building Materials* 22(1):21-29, DOI: 10.1016/j.conbuildmat.2006.09.003

Chen W, Pham TM, Sichembe H, Chen L, Hao H (2018) Experimental study of flexural behaviour of RC beams strengthened by longitudinal and U-shaped basalt FRP sheet. *Composites Part B: Engineering* 134:114-126, DOI: 10.1016/j.compositesb.2017.09.053

Cheng L, Karbhari VM (2006) New bridge systems using FRP composites and concrete: A state-of-the-art review. *Progress in Structural Engineering and Materials* 8(4):143-154, DOI: 10.1002/pse.221

Demin W, Fukang H (2017) Investigation for plastic damage constitutive models of the concrete material. *Procedia Engineering* 210:71-78, DOI: 10.1016/j.proeng.2017.11.050

Dönmez A, Bažant ZP (2017) Size effect on punching strength of reinforced concrete slabs with and without shear reinforcement. *ACI Structural Journal* 114(4):875, DOI: 10.14359/51689719

Ganganagoudar A, Mondal TG, Prakash SS (2016) Analytical and finite element studies on behavior of FRP strengthened RC beams under torsion. *Composite Structures* 153:876-885, DOI: 10.1016/j.compstruct.2016.07.014

Ghobarah A, Ghorbel M, Chidiac S (2002) Upgrading torsional resistance of reinforced concrete beams using fiber-reinforced polymer. *Journal of Composites for Construction* 6(4):257-263, DOI: 10.1061/(ASCE)1090-0268(2002)6:4(257)

Godat A, Neale KW, Labossière P (2007) Numerical modeling of FRP shear-strengthened reinforced concrete beams. *Journal of Composites for Construction* 11(6):640-649, DOI: 10.1061/(ASCE)1090-0268(2007)11:6(640)

Grace NF, Jensen EA, Eamon CD, Shi X (2012) Life-cycle cost analysis of carbon fiber-reinforced polymer reinforced concrete bridges. A*CI Structural Journal* 109(5):697-704, DOI: 10.14359/51684047

Greene Jr GG (2006) Behavior of reinforced concrete girders under cyclic torsion and torsion combined with shear: Experimental investigation and analytical models. Doctoral Dissertation, University of Missouri-Rolla, http://merlin.lib.umsystem.edu/record=b5795688~S5

Hii AKY, Al-Mahaidi R (2006) An experimental and numerical investigation on torsional strengthening of solid and box-section RC beams using CFRP laminates. *Composite Structures* 75(1-4):213-221, DOI: 10.1016/j.compstruct.2006.04.050

Hussain Q, Pimanmas A (2015) Shear strengthening of RC deep beams with openings using sprayed glass fiber reinforced polymer composites (SGFRP): Part 1. Experimental study. *KSCE Journal of Civil Engineering* 19(7):2121-2133, DOI: 10.1007/s12205-015-0243-1

Jumaa GB, Yousif AR (2019) Size effect in shear failure of high strength concrete beams without stirrup reinforced with basalt FRP bars. *KSCE Journal of Civil Engineering* 23(4):1636-1650, DOI: 10.1007/s12205-019-0121-3

Kara IF, Ashour A (2012) Flexural performance of FRP reinforced concrete beams. *Composite Structures* 94(5):1616-1625, DOI: 10.1016/j.compstruct.2011.12.012

Kirane K, Singh KD, Bažant ZP (2016) Size effect in torsional strength of plain and reinforced concrete. *ACI Structural Journal* 113(6): DOI: 10.14359/51689149

Lee SH, Abolmaali A, Shin KJ, Lee HD (2020) ABAQUS modeling for post-tensioned reinforced concrete beams. *Journal of Building Engineering* 30:101273, DOI: 10.1016/j.jobe.2020.101273

Majed MM, Tavakkolizadeh M, Allawi AA (2021) Finite element analysis of rectangular RC beams strengthened with FRP laminates under pure torsion. *Structural Concrete* 22(4):1946-1961, DOI: 10.1002/suco.202000291

Manos GC, Theofanous M, Katakalos K (2014) Numerical simulation of the shear behaviour of reinforced concrete rectangular beam specimens with or without FRP-strip shear reinforcement. *Advances in Engineering Software* 67:47-56, DOI: 10.1016/j.advengsoft.2013.08.001

Mirrashid M, Naderpour H (2021) Recent trends in prediction of concrete elements behavior using soft computing (2010–2020). *Archives of Computational Methods in Engineering* 28:3307-3327, DOI: 10.1007/s11831-020-09500-7

Mohammadi T, Wan B, Harries K (2013) Intermediate crack debonding model of FRP-strengthened concrete beams using XFEM. In Proceedings of the Simulia Community Conference, DOI: 10.13140/RG.2.1.3597.2641

Mondal TG, Prakash SS (2016) Nonlinear finite-element analysis of RC bridge columns under torsion with and without axial compression. *Journal of Bridge Engineering* 21(2):04015037, DOI: 10.1061/%28ASCE%29BE.1943-5592.0000798

Naderpour H, Haji M, Mirrashid M (2020) Shear capacity estimation of FRP-reinforced concrete beams using computational intelligence. *Structures* 28:321-328, Elsevier, DOI: 10.1016/j.istruc.2020.08.076

Naderpour H, Mirrashid M (2020) A novel definition of damage states for structural elements in framed reinforced concrete buildings. *Journal of Building Engineering* 32:101479, DOI: 10.1016/j.jobe.

2020.101479
Obaidat YT, Heyden S, Dahlblom O (2010) The effect of CFRP and CFRP/concrete interface models when modelling retrofitted RC beams with FEM. *Composite Structures* 92(6):1391-1398, DOI: 10.1016/j.compstruct.2009.11.008
Önal MM, Zengin B, Koçak A, Doran B (2014) An experimental investigation on flexural behavior of RC beams strengthened with different techniques. *KSCE Journal of Civil Engineering* 18(7): 2162-2169, DOI: 10.1007/s12205-014-1353-x
Panchacharam S, Belarbi A (2002) Torsional behavior of reinforced concrete beams strengthened with FRP composites. First FIB Congress, Osaka, Japan, DOI: 10.1177/1369433220988625
Pawłowski D, Szumigała M (2015) Flexural behaviour of full-scale basalt FRP RC beams–experimental and numerical studies. *Procedia Engineering* 108:518-525, DOI: 10.1016/j.proeng.2015.06.114
Prakash M, Abishek VL, Abishek R, Devarajan K (2016) Numerical simulation of low velocity impact analysis of fiber metal laminates. *Mechanics and Mechanical Engineering* 20(4):515-530
Raza A, Khan QuZ, Ahmad A (2020) Prediction of axial compressive strength for FRP-confined concrete compression members. *KSCE Journal of Civil Engineering* 24:2099-2109, DOI: 10.1007/s12205-020-1682-x
Sæther I, Sand B (2012) FEM simulations of reinforced concrete beams attacked by corrosion. *ACI Structural Journal* 109(2):15-31, DOI: 10.1088/1757-899X/652/1/012031
Seo SY, Lee MS, Feo L (2016) Flexural analysis of RC beam strengthened by partially de-bonded NSM FRP strip. *Composites Part B: Engineering* 101: 21-30, DOI: 10.1016/j.compositesb.2016.06.056
Sharaky I, Baena M, Barris C, Sallam H, Torres L (2018) Effect of axial stiffness of NSM FRP reinforcement and concrete cover confinement on flexural behaviour of strengthened RC beams: Experimental and numerical study. *Engineering Structures* 173:987-1001, DOI: 10.1016%2Fj.engstruct.2018.07.062
Smith M (2009) ABAQUS/Standard User's Manual, Version 6.9
Teng JG, Lam L, Chen JF (2004) Shear strengthening of RC beams with FRP composites. *Progress in Structural Engineering and Materials* 6(3):173-184, DOI: 10.1002/pse.179
Tibhe SB, Rathi VR (2016) Comparative experimental study on torsional behavior of RC beam using CFRP and GFRP fabric wrapping. *Procedia Technology* 24:140-147, DOI: 10.1016/j.protcy.2016.05.020
Wahalathantri BL, Thambiratnam D, Chan T, Fawzia S (2011) A material model for flexural crack simulation in reinforced concrete elements using ABAQUS. Proceedings of the first international conference on engineering, designing and developing the built environment for sustainable wellbeing, Queensland University of Technology
Yu F, Guan Y, Fang Y, Li D (2021) Experimental and numerical investigations of PVC-FRP confined concrete column-rc beam joint reinforced with core steel tube under axial load. *KSCE Journal of Civil Engineering* 25(12):4671-4685, DOI: 10.1007/s12205-021-0381-6
Yu T, Teng JG, Wong YL, Dong SL (2010) Finite element modeling of confined concrete-II: Plastic-damage model. *Engineering Structures* 32(3):680-691, DOI: 10.1016/j.engstruct.2009.11.013
Zheng YZ, Wang WW, Mosalam KM, Fang Q, Chen L, Zhu ZF (2020) Experimental investigation and numerical analysis of RC beams shear strengthened with FRP/ECC composite layer. *Composite Structures* 246:112436, DOI: 10.1016/j.compstruct.2020.112436
Zhou J, Shen W, Wang S (2017) Experimental study on torsional behavior of FRC and ECC beams reinforced with GFRP bars. *Construction and Building Materials* 152:74-81, DOI: 10.1016/j.conbuildmat.2017.06.131
Zimmermann S (2001) Normal strength concrete in multiaxial compression A 3D constitutive model (including ultimate failure behavior). Report TUE-BCO 01.05, Technische Universiteit Eindhoven, Eindhoven, Niederlande (in German)
Zou X, Lin H, Feng P, Bao Y, Wang J (2021) A review on FRP-concrete hybrid sections for bridge applications. *Composite Structures* 262: 113336, DOI: 10.1016/j.compstruct.2020.113336